





Pre-explosion Spiral Mass Loss of a Binary Star Merger

Ondřej Pejcha^{1,2,3,6} , Brian D. Metzger⁴, Jacob G. Tyles², and Kengo Tomida⁵ 

¹ Institute of Theoretical Physics, Faculty of Mathematics and Physics, Charles University in Prague, Czech Republic; ondrej.pejcha@mff.cuni.cz

² Department of Astrophysical Sciences, Princeton University, USA

³ Kavli Institute of Theoretical Physics, University of California, Santa Barbara, USA

⁴ Columbia Astrophysics Laboratory, Columbia University, New York, NY 10027, USA

⁵ Department of Earth and Space Science, Osaka University, Japan

Received 2017 October 4; revised 2017 October 12; accepted 2017 October 18; published 2017 November 17

Abstract

Binary stars commonly pass through phases of direct interaction, which result in the rapid loss of mass, energy, and angular momentum. Though crucial to understanding the fates of these systems, including their potential as gravitational wave sources, this short-lived phase is poorly understood and has thus far been unambiguously observed in only a single event, V1309 Sco. Here we show that the complex and previously unexplained photometric behavior of V1309 Sco prior to its main outburst results naturally from the runaway loss of mass and angular momentum from the outer Lagrange point, which lasts for thousands of orbits prior to the final dynamical coalescence, much longer than predicted by contemporary models. This process enshrouds the binary in a “death spiral” outflow, which affects the amplitude and phase modulation of its light curve, and contributes to driving the system together. The total amount of mass lost during this gradual phase ($\sim 0.05 M_{\odot}$) rivals the mass lost during the subsequent dynamical interaction phase, which has been the main focus of “common envelope” modeling so far. Analogous features in related transients suggest that this behavior is ubiquitous.

Key words: binaries: close – binaries: eclipsing – stars: evolution – stars: individual (V1309 Sco)

Supporting material: animations

1. Introduction

During some point in their lives, more than a quarter of massive stars, and a comparable fraction of their lower mass brethren, undergo direct interaction with a companion binary star, in a process commonly known as “common envelope” evolution (Sana et al. 2012; Kochanek et al. 2014). Though short-lived and poorly understood, the outcome of this phase has crucial implications for all stages of stellar evolution. The binary components may survive as distinct entities with a reduced orbital separation, leading in some cases to compact object binaries composed of white dwarfs, neutron stars, and black holes. A fraction of these systems will eventually merge through gravitational wave emission, as observed recently with the LIGO and Virgo interferometers (Abbott et al. 2016a, 2016b, 2017). Alternatively, the stellar binary can coalesce completely into a single object with potentially exotic properties. The physical processes at work during the merger that delineate these two outcomes remain one of the biggest unsolved problems of stellar evolution (e.g., Paczyński 1976; Webbink 1984; Livio & Soker 1988; Ivanova et al. 2013b). Mass ejection during the terminal phase of these events can power bright transient emission (Soker & Tylenda 2006; Ivanova et al. 2013a), offering a direct observational window into some of these open issues.

Catastrophic binary interactions have been suggested as an underlying driver for a class of optical transients commonly known as Luminous Red Novae (LRN) or Intermediate Luminosity Optical Transients (ILOT). This modest but growing group includes V838 Mon, V4332 Sgr, OGLE-2002-BLG-360, M31 LRN 2015, M101 OT2015-1, and NGC 4490 OT2011 (e.g., Soker & Tylenda 2003; Tylenda & Soker 2006; Tylenda et al. 2013; Kurtenkov et al. 2015; Williams

et al. 2015; Smith et al. 2016; MacLeod et al. 2017; Mauerhan et al. 2017). The case for binary interaction as the origin of LRN/ILOT was significantly strengthened with the discovery of V1309 Sco, where the archival OGLE photometry revealed a contact binary with a decaying orbital period that was followed by a luminous outburst (Tylenda et al. 2011). Below we review the pre-outburst evolution of V1309 Sco and outline the structure of this paper.

1.1. Overview of V1309 Sco Light Curve

V1309 Sco was discovered near the peak of its outburst in 2008 September (Figure 1) and was soon spectroscopically recognized as a member of LRN (Mason et al. 2010). Archival observations of V1309 Sco, primarily from the OGLE survey, revealed a contact eclipsing binary with an orbital period $P \approx 1.4$ days, total mass $M = 1\text{--}2 M_{\odot}$, effective temperature 4500 K, and luminosity $L_{\text{binary}} \approx 10 L_{\odot}$, as measured ≈ 7 years prior to the outburst (Tylenda et al. 2011). Between 2001 and 2007, the orbital period of V1309 Sco decayed rapidly, with a timescale P/\dot{P} that decreased from about 1000 to 170 years, with a total decrease in the period over this interval of $\sim 1\%$ (Pejcha 2014; Tylenda et al. 2011). The measured acceleration timescale \dot{P}/\ddot{P} of a few years greatly exceeded the orbital period of the binary, yet was much shorter than the timescale for tidally induced orbital decay (Pejcha 2014). Simultaneously with this period decay, the phased light curve gradually morphed from a double-hump profile (typical for contact binaries) to a single-hump shape (Figure 2) as the mean brightness increased by about 1 mag (Figure 1). This transformation occurred gradually over thousands of orbits, during which time the binary separation shrank by only $\sim 1.5\%$. Earlier work attributed this transformation to the appearance of hot spots on the binary surface (Tylenda et al. 2011); however, given freedom on the number of spots, as well as their sizes,

⁶ Lyman Spitzer Jr. Fellow.

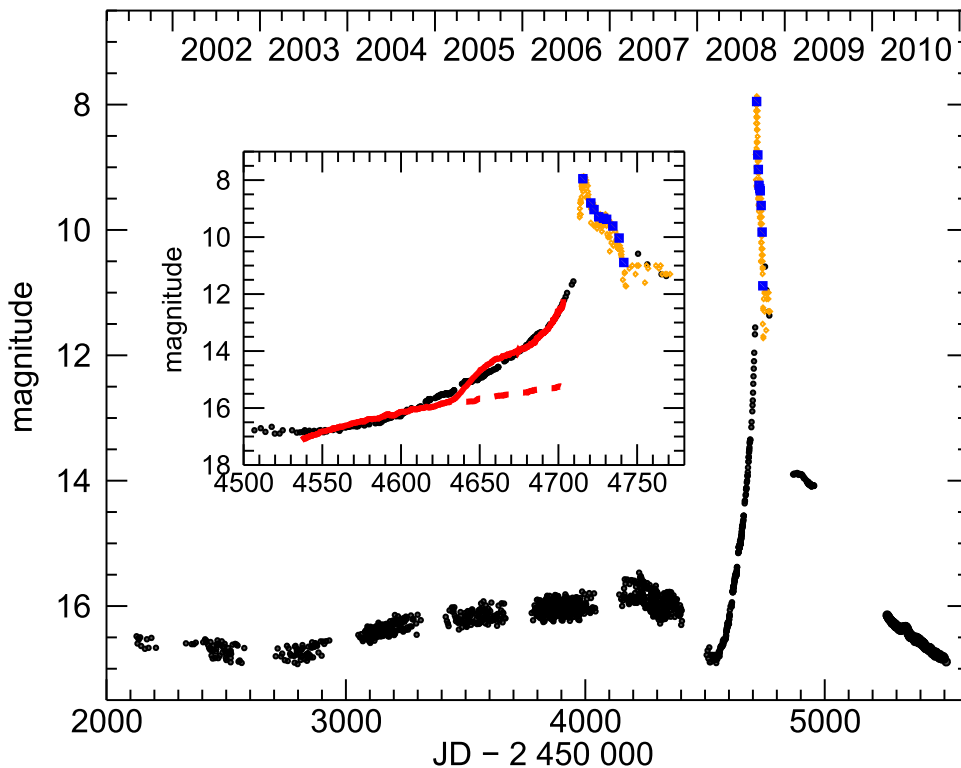


Figure 1. Light curve of V1309 Sco. Black points show *I*-band observations from OGLE (Tylenda et al. 2011); blue squares show *V*-band magnitudes from ASAS Pojmanski (1997); and orange points show visual magnitudes from AAVSO (Kafka 2017). The inset plot shows the observed gradual rise of brightness compared with bolometric light curves $-2.5 \log L_{\text{bol}}$ from our three-dimensional SPH simulations, both with (solid red) and without (dashed red) accounting for evolution of the particle injection temperature. The simulated light curves are offset by an arbitrary constant to roughly match the observed magnitude at the onset of the slow brightening. The luminosity from the simulation ($20 L_{\odot}$) roughly matches the inferred luminosity of V1309 Sco binary ($10 L_{\odot}$) around the epoch JD 2 454 550 (Tylenda et al. 2011; Tylenda & Kamiński 2016).

temperatures, and time evolution, this phenomenological model can reproduce almost any light curve shape. Here we present an alternative explanation with fewer free parameters, which naturally explains other puzzling features of V1309 Sco.

During the second half of 2007, V1309 Sco began to fade, and around the same time its orbital-timescale variability ceased. Then, over the first 8 months of 2008, the system gradually brightened by $\gtrsim 5$ mag, on a timescale which, while still much longer than the orbital period, was comparable to the period acceleration timescale \dot{P}/P . Such a slow rise is perhaps unexpected: the initial rise time of “explosive” astrophysical transients is usually fast, similar to the radial expansion timescale of the ejecta. Finally, in early 2008 September, V1309 Sco brightened by an additional 3 mag to its peak in just a few days. The subsequent ~ 20 day long plateau was interpreted as emission produced by hydrogen recombination, following the ejection of $0.04\text{--}0.09 M_{\odot}$ from the binary (Ivanova et al. 2013a; Nandez et al. 2014).

1.2. Outline of the Paper

Although the physical mechanism responsible for driving V1309 Sco to merge was attributed to the tidal Darwin instability (Rasio 1995; Stępień 2011; Nandez et al. 2014), this alone cannot account for the complex evolution of the binary orbital period, phased light curve, and mean brightness. It is also unclear how the final dynamical event was triggered: what, precisely, was so special about the point at which the binary evolution became dynamical, given that

preceding changes to the orbit and structure occurred gradually of thousands of orbits? We will argue that mass-loss from the outer Lagrange point of the binary L_2 likely plays the dominant role in this behavior. L_2 mass loss was previously invoked to explain the pre-maximum behavior of V1309 Sco (Tylenda et al. 2011; Tylenda & Kamiński 2016), and was shown to work at the order-of-magnitude level (Pejcha 2014).

In Section 2 we review the physics of L_2 mass loss and describe our radiation hydrodynamic simulations with realistic microphysics. We show that by postulating mass loss occurred from L_2 at a progressively increasing rate \dot{M} leading up to the dynamical phase, one can account for the full sequence of behavior observed in V1309 Sco quantitatively, in detail, and with a smaller number of free parameters than previous models. In Section 3 we show that the observed changes in the phased light curve due to obscuration by the mass loss streams are consistent with the same mass loss required to explain the period decay. Then in Section 4 we argue that the slow brightening toward maximum at later times is naturally explained as a continuation of the runaway behavior of \dot{M} . Based on the results of our simulations, we speculate that what defined the final dynamical event was the critical point at which the binary had lost most of its angular momentum through L_2 outflow. Given that V1309 Sco represents the best studied member of its class, the ramifications from our results may extend to the broader class of transients resulting from stellar mergers, and more broadly to the theory of catastrophic binary interactions, as we discuss in Section 5.

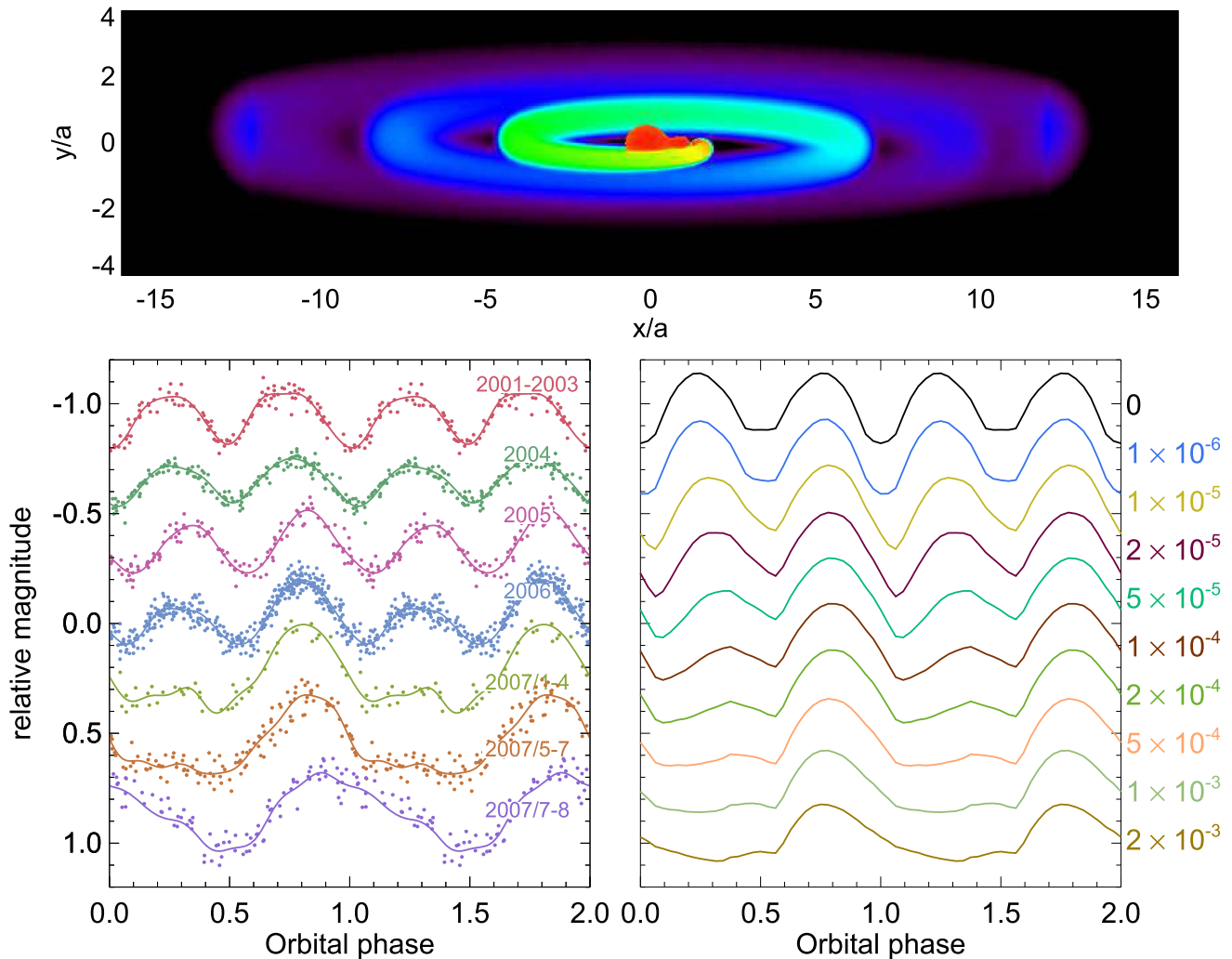


Figure 2. Phased light curves of a V1309 Sco. (Lower left) Observed evolution from OGLE phased according to the time-changing orbital period (Tylenda et al. 2011). (Lower right) Theoretical light curves accounting for obscuration by the L_2 stream, constructed for a binary of mass $M = 1.65 M_\odot$, mass ratio $q = 0.1$, and semimajor axis $a = 0.03$ au, viewed at an inclination of $i = 84^\circ$. Colors distinguish different values of the mass-loss rate \dot{M} , labeled in units of $M_\odot \text{ yr}^{-1}$. Light curves are offset vertically for purposes of clarity. (Top) Example ray-traced image showing the binary partially obscured by the L_2 stream.

(An animation of this figure is available.)

2. L_2 Mass Loss

L_2 mass loss was originally introduced as a natural outcome of a wide range of binary evolution pathways (Webbink 1976; Flannery & Ulrich 1977; Livio et al. 1979). However, because of the common belief that the two stellar components cannot maintain complete corotation with the orbit, frictional drag in a “common envelope” has been instead invoked as the main physical process responsible for tightening the binary orbit (Paczynski 1976; Meyer & Meyer-Hofmeister 1979; Ivanova et al. 2013b; MacLeod & Ramirez-Ruiz 2015). Some numerical hydrodynamical simulations find L_2 mass loss, but only in the few final orbits before the dynamical interaction, especially in cases when the binary begins in synchronous rotation (Rasio & Shapiro 1995; Lombardi et al. 2011; Nandez et al. 2014).

We consider the following scenario to explain V1309 Sco. We suggest that V1309 Sco was initially a contact binary, which increased its fillout factor due to the primary evolving off of the main sequence or due to the shrinking of the orbit by the Darwin instability triggered by secular decrease of the mass ratio due to thermal relaxation oscillations. The structure of the binary was not markedly different from other field contact

binaries—in particular, the stars were in corotation with the orbit. This is consistent with the phased light curve in 2001–2003, relatively slow initial orbital period change consistent with tidal timescale, and the existence of other stable contact binaries with similar orbital period (e.g., Pawlak et al. 2013). When the expansion of the binary surface reaches the outer critical surface, the binary starts losing mass from L_2 .⁷ We postulate that the gas is launched at corotation from L_2 and that the timescale of angular momentum loss is much longer than the orbital period. We note that, empirically, synchronous rotation appears to be an excellent assumption in V1309 Sco because of its nearly constant orbital period observed for several years prior to the merger by OGLE. Whether the mass lost through L_2 comes from the lighter star or is first transferred from the heavier one to the lighter one is not clear, but this uncertainty is included in the following discussion.

⁷ In principle, similar setting can occur in normal mass transfer through L_1 , when the secondary cannot accept the mass and inflates, forming an object that presumably looks similar to a contact binary, as was considered, for example, by Livio et al. (1979).

Table 1
Explanation of Parameters Used in This Work

| Parameter | Explanation | Value or Comment |
|--------------------------------|--|---|
| M_1 | Mass of the lighter star | $0.15 M_\odot$ for phased light curve, $\dot{M}_1 \equiv \dot{M}$ for gradual rise to maximum |
| M_2 | Mass of the heavier star | $1.5 M_\odot$ |
| q | Mass ratio | M_1/M_2 |
| a | Semimajor axis | 0.03 au for phased light curve, for gradual rise to maximum calculated from Equation (2) |
| P | Orbital period | Calculated from Kepler law or Equation (2) |
| v_{orb} | Orbital velocity | $\sqrt{GM/a}$ |
| v_{esc} | Escape velocity | $\sqrt{2GM/a}$ |
| t | Time | |
| E | Orbital energy | $-GM_1M_2/(2a)$ |
| $\mathcal{E}_i, \mathcal{E}_f$ | Initial and final energy (sum of potential and kinetic) of a corotating test particle at L_2 in units of GM/a | Equation (1) |
| \mathcal{A} | Conversion between \dot{P}/P and \dot{M}/M ; depends only on q (Pribulla 1998) | Typical values 30–50 for $q = 0.1$, Equation (2) |
| f | Additional angular momentum extracted from the binary orbit by a particle released from L_2 and moving to infinity | Assumed mostly 1.2, Equation (2) |
| ε | Initial width of L_2 stream | 0.01 in SPH calculations, roughly proportional to c_S/v_{orb} (Shu et al. 1979) |
| ρ_{center} | Density at the center of L_2 stream | Equation (4) |
| ψ | Perpendicular distance from the L_2 stream center | In units of a , Equation (5) |
| T_{binary} | Photospheric temperature of the binary | 4500 K, Equation (6) |
| I | Intensity along a ray | Equation (7) |
| s | Distance along a ray | Equation (7) |
| κ | Opacity | Equation (7) |
| i | Inclination | Preferred value is 84° , given the assumed density profile of the L_2 stream |
| φ | Orbital phase | Obtained by integrating $1/P$ |
| t_0 | Time of singularity in \dot{M} | Corresponds roughly to the main peak, Equation (9) |
| δ | Exponent of runaway of \dot{M} | “Best-fit” value 3, Equation (9) |
| T_{in} | Injection temperature of particles at L_2 | Equation (10) |
| $T_{\text{in},0}$ | Initial injection temperature of particles at L_2 | Equal to T_{binary} , Equation (10) |
| \dot{M}_T | Critical \dot{M} , above which T_{in} begins to increase | “Best-fit” value of $10^{-2} M_\odot \text{ yr}^{-1}$, Equation (10) |
| γ | Exponent of runaway of T_{in} | “Best-fit” value 0.5, Equation (10) |
| b_j, c_j | Coefficients of Fourier expansion of phased light curve | Section 3.1 |

In this section, we briefly review the physics of L_2 mass loss and describe our calculation of various quantities. We summarize our nomenclature in Table 1.

2.1. Brief Overview of Previous Results

The physics of L_2 mass loss are conceptually similar to the more commonly studied case of mass transfer through the inner Lagrange point. Considering the ballistic motion of cold matter, the spiral stream produced by matter leaving in corotation from L_2 experiences tidal torques from the binary and gains sufficient energy to become unbound for binary mass ratios $0.064 \leq q \leq 0.78$, reaching asymptotic velocities up to $\sim 25\%$ of the binary escape velocity. Mass loss from binaries with mass ratios outside of this range instead was predicted to form a bound circumbinary disk (Shu et al. 1979). Using three-dimensional smoothed-particle hydrodynamic simulations, including the effects of radiative cooling and diffusion, we recently showed that L_2 mass-loss can lead to qualitatively different outcomes, depending on the stellar surface temperature (initial temperature of matter at L_2) and cooling efficiency, in addition to the binary mass ratio (Pejcha et al. 2016b). In cases that produce unbound streams, internal shocks between the merging spiral arms power a substantial

luminosity L_{stream} in excess of that originating from the surface of the binary star (Pejcha et al. 2016a).

2.2. Energetics of L_2 Mass Loss

Test particles positioned at L_2 , which are corotating with the binary, always possess a negative sum of kinetic and gravitational potential energies. When matter starts moving out on a ballistic trajectory, tidal torques from the time-changing gravitational field of the binary increase the total energy, such that the final asymptotic energy is positive for a wide range of binary mass ratios, $0.064 < q < 0.78$. This energy loss from the binary orbit \dot{E}_{L_2} , mediated by gravitational field, can be expressed as

$$\frac{\dot{E}_{L_2}}{E_{\text{orb}}} = \left[-2(\mathcal{E}_f - \mathcal{E}_i) \frac{(1+q)^2}{q} \right] \frac{\dot{M}}{M}, \quad (1)$$

where $E_{\text{orb}} = -GM_1M_2/(2a)$ is the energy of the orbit, and $\mathcal{E}_f - \mathcal{E}_i$ is the difference between initial and final energy of test particle in units of GM/a ; $\mathcal{E}_i < 0$ for all q in corotation, $\mathcal{E}_f > 0$ for $0.064 < q < 0.78$ (Shu et al. 1979). Using previous analytic calculations (Shu et al. 1979), the term in square brackets has a numerical value of -4.48 for $q = 0.1$.

At the same time, the loss of angular momentum from L_2 and the requirement of circular orbit imply that the orbital period will decrease accordingly as

$$\frac{\dot{P}}{P} = f \mathcal{A} \frac{\dot{M}}{M}, \quad (2)$$

where \mathcal{A} is a constant reflecting the specific angular momentum of the L_2 point, which depends on q and which of the two stars is actually losing mass (Pribulla 1998), and f is a factor representing the additional angular momentum extracted from the binary by tidal torques. We choose a value of $f = 1.2$ based on our previous results (Pejcha et al. 2016a), although this is close to the maximum allowed value (Shu et al. 1979). Together with the third Kepler law, this angular momentum loss implies a corresponding orbital energy loss:

$$\frac{\dot{E}_{\text{orb}}}{E_{\text{orb}}} = \left[\frac{1+q}{q} \frac{\dot{M}_1}{M} + (1+q) \frac{\dot{M}_2}{M} - \frac{2}{3} f \mathcal{A} - \frac{1}{3} \right] \frac{\dot{M}}{M}. \quad (3)$$

For $q = 0.1$ and a fiducial value of $f = 1.2$, we find that the term in square brackets takes on values of -9.6 and -43 for cases when the total mass loss occurs entirely from the lighter ($\dot{M}_1 = \dot{M}$) or heavier star ($\dot{M}_2 = \dot{M}$), respectively. Even for $f = 1$, the coefficient values are -6.2 or -36 , respectively.

These results imply that the loss of binary orbital energy is more than enough to unbind material through L_2 mass loss. Most of the energy gain $\mathcal{E}_f - \mathcal{E}_i$ experienced by gas flowing out of L_2 is used on countering the gravitational potential well. The asymptotic kinetic energy is at most $\sim 30\%$ of the total energy gain $\mathcal{E}_f - \mathcal{E}_i$. However, for $q = 0.1$ it is only 7% (Shu et al. 1979).

The remaining released orbital energy, which was not expended on unbinding and accelerating the outflowing mass by tidal torques, presumably goes to heating and expansion of the stars, as well as the kinetic energy of bulk motions in the stellar surface layers. Additional work is needed to fully understand the partitioning of the orbital energy, which ultimately powers the envelope mass ejection.

2.3. Smoothed-particle Hydrodynamics (SPH) of L_2 Mass Loss

Our numerical simulations of L_2 mass loss were conducted with a custom SPH code developed to study dynamics and radiative properties of outflows from binary stars (Pejcha et al. 2016a, 2016b). The problem is set up by continuously injecting particles with a specified temperature T_{in} in a small vicinity of the L_2 point with an initially Gaussian density profile perpendicular to the binary axis. The initial Gaussian width $\varepsilon = c_S/v_{\text{orb}}$ is roughly set by the ratio of the stellar surface sound speed c_S and orbital velocity v_{orb} (Shu et al. 1979), and we have verified our results are insensitive to the value of ε as long as it is sufficiently small. We use $\varepsilon = 0.01$ as our fiducial value. Particles that cross back inside of L_2 are removed from the simulation domain; particles are adaptively injected to ensure that total active mass in the simulation corresponds to total mass lost from the binary. In the case of a time-dependent \dot{M} , we vary the mass of injected particles to maintain specified particle injection rate, which sets the numerical resolution of the simulation. Since we primarily study unbound L_2 outflows, all particles within a smoothing volume were typically ejected around the same time and have similar mass.

The particles are initially in corotation with the L_2 point, and their acceleration is calculated using standard hydrodynamical and viscous forces with adaptive smoothing length. Gravitational forces from the binary star are modeled as a combination of two point masses, M_1 and M_2 , with total mass $M = M_1 + M_2$, mass ratio $q = M_1/M_2$, semimajor axis a , and orbital period P . Self-gravity between the particles is neglected.⁸ The energy evolution includes hydrodynamic and viscous terms, flux-limited radiative diffusion, and radiative cooling (Stamatellos et al. 2007; Forgan et al. 2009). Calculations relevant for the phased light curve evolution also include irradiation by the central binary, which we model as three point sources positioned at the barycenter, and slightly above and below to better capture vertical extent of the source. The implementation of these effects, equation of state, opacities, and estimates of luminosity and effective temperature are mostly identical to our previously published works (Pejcha et al. 2016a, 2016b). Even our approximate implementation of the relevant radiative processes results in an outflow temperature structure, which is coupled to the radiation and is therefore significantly more realistic than what would be obtained from a purely adiabatic treatment. This allows us to obtain phased light curves by post-processing the simulation data, detailed as follows.

2.4. Calculation of Phased Light Curves

In order to build our understanding of how the phased light curve of the binary changes when viewed through the L_2 stream, we constructed a semi-analytic model of the problem. We calculate the trajectory of the stream center, as well as the velocity v and the evolution of perpendicular stream spread ϵ (Shu et al. 1979), which therefore also gives the density at the stream center,

$$\rho_{\text{center}} = \frac{\dot{M}}{2\pi\epsilon^2v}. \quad (4)$$

The density profile moving away from the stream center is assumed to obey

$$\rho(\psi) = \rho_{\text{center}} \exp\left(-\frac{\psi^2}{2\epsilon^2}\right), \quad (5)$$

where ψ is the distance from a given position to the closest point on the stream center trajectory. The temperature along the stream center is set by irradiation from the binary,

$$T = T_{\text{binary}} \sqrt{\frac{r_{L_2}}{r}}, \quad (6)$$

where r_{L_2} is the distance of the L_2 point from the barycenter; a fixed temperature is assumed for all values of ψ . The stream is truncated at the radius r_{coll} , where consecutive spiral arms collide, which is one of the free parameters of the model with a default value of $8a$, as motivated by the collision radius seen in our simulations (Pejcha et al. 2016a). The density profile outside of r_{coll} is assumed to be an axially symmetric wind with

⁸ A simple comparison between the timescale for gravitational collapse and that of outflow expansion suggests that the gas will not form a gravitationally bound substructure (Pejcha et al. 2016a). Thermal instability is a more promising way to form clumps in the outflow, which together with associated changes in the opacity provides a possible explanation for the small-scale ‘‘wiggles’’ that occur during the rising phase of the light curve (Pejcha 2014; Pejcha et al. 2016a).

constant \dot{M} ($\rho \sim r^{-2}$) and opening angle set to match the value of ϵ at the radius of the collision. We neglect contributions to the luminosity that arise from the collision of the spiral streams, because at times of interest we find that the collision luminosity is at most comparable to the binary luminosity; furthermore, the low value of $T_{\text{eff}} \approx 2000\text{--}3000$ K of this emission (due to the large collision radius) will suppress its contribution to the optical bands for \dot{M} achieved before 2008. With these informed choices, we find a remarkably accurate match to the density and temperature profile of matter surrounding the binary compared with more complete SPH calculations.

The appearance of the binary surrounded by the L_2 mass loss stream is constructed by semi-implicitly integrating the intensity I along parallel rays according to the standard radiative transfer equation,

$$I(s + ds) = e^{-\kappa_{\text{eff}} ds} I(s) + (1 - e^{-\kappa_{\text{eff}} ds}) S(s), \quad (7)$$

where s is measured along the ray and $S(s)$ is the source function. The latter we assume to obey either $S \propto T^4$ when obtaining the bolometric light curve, or the Planck law $S = B_{\lambda}(T)$ when considering the emission at specific wavelengths. The results shown for V1309 Sco are calculated for I band at $\lambda = 800$ nm, corresponding to the OGLE observations. We assume that the opacity of gas with hydrogen mass fraction $X = 0.7$ and metallicity $Z = 0.02$ is given by the approximate expression

$$\kappa = \kappa_{\text{m}} + (\kappa_{\text{H}^-}^{-1} + (\kappa_{\text{e}} + \kappa_{\text{K}})^{-1})^{-1}, \quad (8)$$

where $\kappa_{\text{m}} = 0.1Z$ is an approximate molecular opacity, $\kappa_{\text{H}^-} = 1.1 \times 10^{-25} Z^{0.5} \rho^{0.5} T^{7.7}$ is the H^- opacity, $\kappa_{\text{e}} = 0.2(1 + X)$ is the electron scattering opacity, and $\kappa_{\text{K}} = 4 \times 10^{25} (1 + X) Z \rho T^{-3.5}$ is the Kramers opacity, all in cgs units. The default opacity for $r > r_{\text{coll}}$ is $\kappa_{\text{wind}} = \kappa_{\text{m}}$, but we investigate both larger and smaller values in order to study, in a heuristic manner, effects such as dust formation.

The rays are cast on a regular grid, the orientation of which we vary relative to the binary orbital plane to study the appearance of the system from different inclinations i and phase angles φ . If a ray intersects the outer critical surface of the binary, we initiate the integration of Equation (7) at this point with initial temperature 4500 K and take into account linear limb darkening law, where we use the angle between the ray and the normal to the outer critical surface. If a ray does not intersect the binary surface, we put the starting point on the far side of the binary with intensity initially set to zero.

2.5. Calculation of Gradual Brightening

When directly simulating the final gradual rise toward the maximum, the parameters of the binary will significantly change due to the loss of mass and angular momentum. We prescribe the time evolution $\dot{M}(t)$ as a power-law approach to a singularity (Webbink 1977; Pejcha 2014),

$$\dot{M}(t) = \dot{M}_0 \left(\frac{t_0}{t_0 - t} \right)^{\delta}. \quad (9)$$

As discussed in detail later, we find that in order to match the light curve, we need to eventually increase the injection temperature of the particles T_{in} . We assume that $T_{\text{in}}(t)$

evolves as

$$T_{\text{in}}(t) = \begin{cases} T_{\text{in},0} & \dot{M}(t) < \dot{M}_T \\ T_{\text{in},0} \left(\frac{\dot{M}(t)}{\dot{M}_T} \right)^{\gamma} & \dot{M}(t) \geq \dot{M}_T. \end{cases} \quad (10)$$

We vary the parameters \dot{M}_0 , t_0 , δ , \dot{M}_T , and γ to match the observed light curve. $T_{\text{in},0}$ is set to 4500 K.

The loss of angular momentum is self-consistently included using the rate of L_2 mass loss according to Equation (2). We experimented with several choices for the value of \mathcal{A} , corresponding to the assumption that one of the stars carried all of \dot{M} ; \dot{M} was split equally between the stars; or the mass loss was such that q remains constant. Each possibility gave similar results to within a factor of $\lesssim 2$. In the end, we choose to assign all of the mass loss to the lighter star, which produces the smallest change of orbital period for a given value of \dot{M} (Pribulla 1998). Although the mean density of the lighter star is higher, it might be very centrally condensed with small density in the envelope (Paczynski et al. 2007). More work is needed to understand which star is ultimately losing mass in this case. The orbital phase φ of the binary is simultaneously integrated as $\dot{\varphi} = 1/P$. The luminosity produced by the outflow is a sum of the radiative cooling rate of all particles.

3. Changes in the Phased Light Curve

In this section, we describe how runaway L_2 mass loss explains the evolution of the phased light curve of V1309 Sco.

3.1. Results

Figure 2 shows how the phased light curve of the binary changes when viewed through the L_2 mass loss stream, a “death spiral” with nearly edge-on inclination. In isolated binaries, the transit of the smaller, less massive secondary in front of the larger, more massive primary is observed as the primary eclipse (phase 0). After this point, the visible surface area of the binary increases and reaches a maximum at phase 0.25. However, in this case the L_2 stream trails behind the secondary and obscures the binary light, leading to a suppression of the maximum at phase 0.25. Half a period later (phase 0.75), when the binary surface area again reaches maximum, the L_2 stream is less opaque and positioned farther away from the binary, such that the observed flux at this phase is closer to its original, unattenuated value. The strength of this asymmetric effect increases as \dot{M} rises in time, naturally explaining the transformation of the V1309 Sco light curve from double- to single-humped.

We illustrate this transformation of the phased light curve quantitatively in the middle panel of Figure 3 for a range of binary inclinations and r_{coll} . We first decomposed the theoretical light curves in harmonic sine and cosine waves with amplitudes (b_j, c_j) , and then calculated the ratio of second to first harmonic $\sqrt{(b_2^2 + c_2^2)/(b_1^2 + c_1^2)}$. For contact binary with two maxima per period, the second harmonic dominates leading to very high values of the parameter. As the asymmetry due to obscuration by the L_2 stream becomes stronger, the first harmonic comes to dominate, as seen in Figure 3. At the same time, the light curve amplitude changes only slightly for greater inclination angles, for which the obscuring effect dominates.

The stream intersects the sight line with the binary for inclination angles $i \gtrsim 70^\circ$, and results in complete obscuration

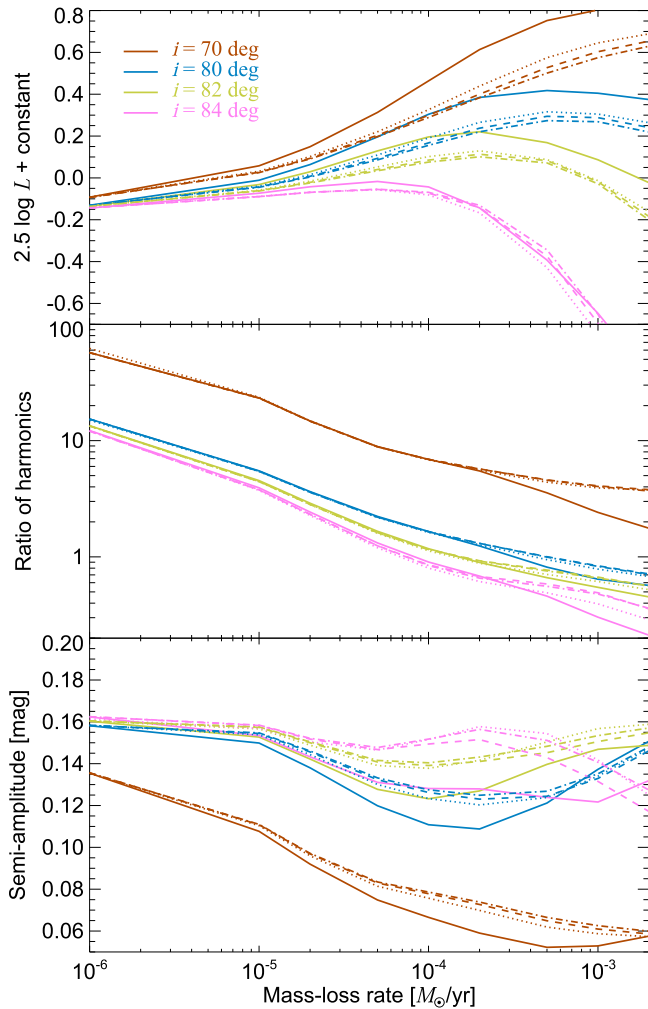


Figure 3. Changes of observable quantities of phased light curves within our semi-analytic model as a function of \dot{M} : mean flux evaluated at 800 nm (top), ratio of amplitudes of the second and first harmonics of the Fourier decomposition of the light curves (middle), and the semi-amplitude in magnitudes (bottom). Colors indicate the range of inclination angles, as shown in the legend in the top panel, and line styles denote different values of r_{coll} of $6a$ (solid), $8a$ (dotted), $10a$ (dashed), and $12a$ (dotted-dashed).

for $i \gtrsim 85^\circ$ (see also Section 3.2). The lower limit on i , required to explain the light curve phase evolution, breaks the degeneracy between the inclination and mass ratio in light curves of contact binaries (Rucinski 1993, 2001), constraining the mass ratio of V1309 Sco to be $q \lesssim 0.1$, given the observed amplitude of the light curve variation in 2001. A lower limit on the mass ratio of $q \gtrsim 0.07$ can also be placed by requiring that the L_2 spiral stream does not form a bound circumbinary disk, which instead would result in a much higher radiative efficiency than observed.

As \dot{M} grows, the additional contribution from radiative cooling of the L_2 stream initially increases the total luminosity of the system. However, this trend temporarily reverses once the central binary becomes almost completely obscured, after which point an even larger value of \dot{M} further attenuates the luminosity. We illustrate this quantitatively in the top panel of Figure 3. Similar gradual brightening followed by subsequent dimming was observed in V1309 Sco in 2001–2007, although the total amplitude of this effect in our models is smaller than that observed. A detailed comparison between the theory and the data on V1309 Sco is shown in Figure 4. Part of the

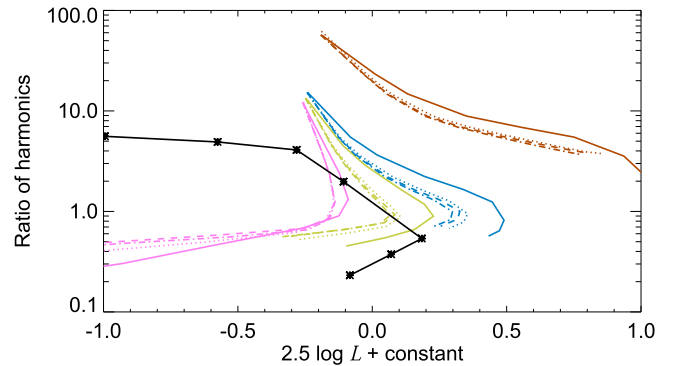


Figure 4. Correlation between the mean flux and the ratio of amplitudes of second and first harmonics from Figure 3. The black points connected by lines indicate the same quantities obtained from the 2001–2007 OGLE light curves of V1309 Sco. To obtain these points, we first fitted the light curve with a spline to determine long-term flux variations. Next, we subtracted these variations and analyzed the phased light curves. For each line, the evolution in time proceeds from top to bottom.

discrepancy might be due to changes in the surface temperature and luminosity of the binary as it undergoes rapid mass stripping, a possibility we investigate in Section 4.2.1.

3.2. Parameter Dependence and Degeneracies

Except for small systematic offsets, the general evolution of the light curve, in particular its transformation from a double-to single-humped profile shown in Figure 2, does not depend on the stream collision radius r_{coll} (Figure 3). The secular increase in the mean observed flux depends on the assumed stream cooling efficiency. The subsequent dip in the flux depends on the wind opacity κ_{wind} , but is present even in the limit that $\kappa_{\text{wind}} = 0$.

Thus far we have neglected the presence of dust along the path of the outgoing light from the binary. However, because the dust opacity $\kappa_{\text{dust}} \gg \kappa_{\text{m}}$, even a moderate amount of dust formation would completely obscure the central area. A simple estimate, based on requisite conditions for dust condensation and coagulation, suggests that dust formation should be copious in the outflow, given its density and expansion rate predicted by our model (Pejcha et al. 2016a, 2016b). However, the process of dust formation in this setting is particularly complex and is controlled by the interplay between rapid expansion, shocks from spiral collisions, and irradiation by the central binary, all of which are treated primitively in our model. Consistency with the observations in fact only requires that dust formation be suppressed in the irradiated “skin” of the outflow, at radii within a few tens of a (dust can still form in the orbital plane, where it would not directly obscure the central regions). Such a picture agrees with modeling of the optical to infrared spectral energy distribution in 2007, for which the optical depth to the star was inferred to be < 1 , but a better fit to the observations is obtained if the material is arranged in a disk-like structure with a small vertical aspect ratio (Tylenda & Kamiński 2016). Regardless of these issues, dust formation probably cannot be avoided once the stream self-obscures and the binary variability vanishes ($\dot{M} \gtrsim 10^{-3} M_\odot \text{ yr}^{-1}$ or after JD 2 454 500 in V1309 Sco). After this point, we are primarily observing light that is generated by the spiral stream collisions well outside of the central star.

A degeneracy exists between three quantities that control the light curve appearance: \dot{M} , i , and κ . Our assumed opacity

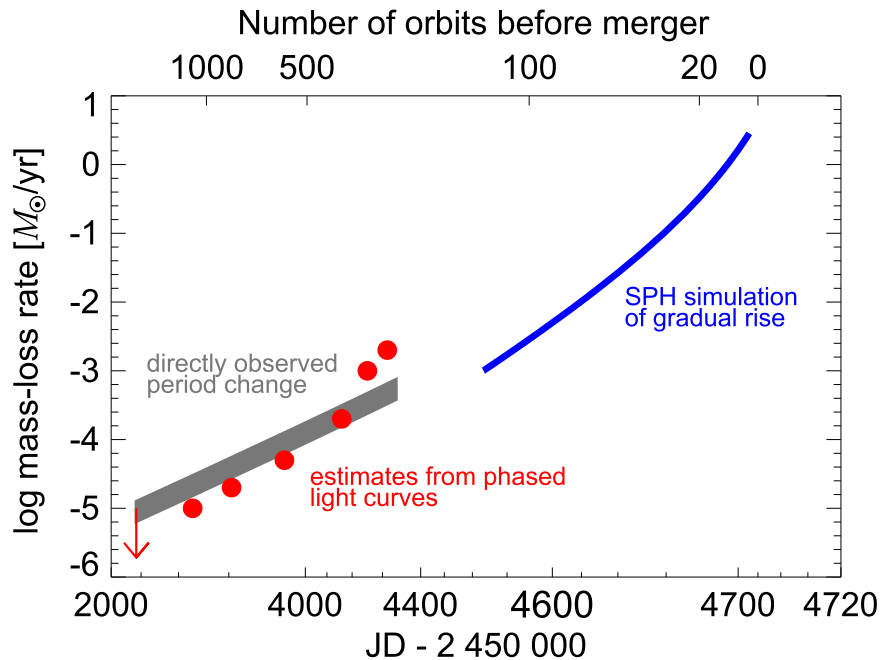


Figure 5. Time evolution of the mass-loss rate in V1309 Sco derived from (1) the directly observed orbital period change, assuming a binary mass ratio $0.07 \leq q \leq 0.1$ (gray line); (2) the visual comparison of theoretical and observed phased light curves in Figure 2 (red circles); and (3) simulations that reproduce the gradual slow luminosity rise to the maximum (blue line). The approximate number of orbits remaining until the merger is indicated on the top axis. The width of the gray line includes uncertainties in assigning \dot{M} to either star in the binary as well as those on the value of q . Sensitivity to the parameters and their degeneracy are discussed in Section 3.2.

roughly corresponds to the Rosseland mean, but this should be regarded as a lower limit, because for values of \dot{M} of interest, the stream is not fully optically thick. It is then easy to imagine that more appropriate band-integrated opacity would be a factor of a few times higher than the Rosseland mean (Alexander & Ferguson 1994). As a result, the value of \dot{M} that we infer from the phased light curve may be somewhat overestimated. On the other hand, a higher value of \dot{M} would move the isodensity contours further from the orbital plane, such that the binary light curve will be noticeably affected even for smaller values of i than needed in our fiducial model. Here, reasonable values of \dot{M} imply we are viewing V1309 Sco at $80^\circ \lesssim i \lesssim 85^\circ$, but this depends sensitively on what we assume for the density profile perpendicular to the stream trajectory. Without a detailed simulation of the stellar surface near L_2 , one can only hypothesize the possible range of outcomes—for instance, if the density profile decreases shallower than the Gaussian profile we have assumed, then the allowed range of i will be greater. In all cases, however, the stream geometry requires a minimum value of $i \gtrsim 70^\circ$, such that similar behavior to that of V1309 Sco should be observed in up to $\sim 1/3$ of randomly oriented binaries. As a result, some freedom exists in the value of \dot{M} required to reproduce the phased light curves (Section 3.3).

We have also explored calculating phased light curves directly from our SPH simulations. Although we obtain qualitatively similar results to the procedure described previously, the simulations suffer from poor resolution away from the stream center and artifacts near the injection point. Furthermore, the simulation must be run for a long time to overcome the initial transient (which lasts tens of orbits in some cases), because the explicit timestep is very short due to radiative diffusion and cooling (Pejcha et al. 2016a).

3.3. Comparison with Directly Observed Orbital Period

The specific angular momentum extracted from the binary provides a direct link between the mass-loss rate \dot{M} and the orbital period change \dot{P} (Pribulla 1998; Pejcha 2014) (Equation (2)). Figure 5 compares the evolution of $\dot{M}(t)$ as inferred from the observed orbital period change to that required to reproduce the morphological changes observed simultaneously in the phased light curve. The good agreement between these two independent methods suggests that the orbital period change was driven primarily by L_2 mass loss, at least at late times. However, we cannot exclude the possibility that in the earliest phases (2001–2003) angular momentum loss was instead dominated by other processes, such as the Darwin tidal instability.

4. Gradual Rise to Maximum

We hypothesize that nothing particularly dramatic occurred to V1309 Sco near the end of 2007; the system variability simply vanished once the binary surface became completely blocked by the L_2 mass loss stream. After this point, the observed emission was dominated by shocks internal to the L_2 outflow instead of the binary surface. Although near the end of 2007 the shock luminosity was comparable to that of the binary ($L_{\text{binary}} \approx L_{\text{stream}}$), the low temperature of the shock emission ($\lesssim 3000$ K (due to its comparatively large radius) resulted in a temporary decrease in the I band luminosity. The agreement between the predictions of our model and the observed binary evolution at low \dot{M} motivates us to extend it to even higher mass loss rates. In this section, we directly simulate the last ~ 200 days of evolution with our SPH code, assuming that the mass loss rate $\dot{M}(t)$ continues the runaway evolution inferred earlier, and then compare our results with the observed rising light curve prior to the dynamical phase.

4.1. Results

Initially we experimented with varying only the parameters that describe \dot{M} (Equation (9)) while keeping the matter ejection temperature T_{in} (Equation (10)) fixed. However, we found a limit to the amount of upward *curvature* that can be obtained in the light curve rise: no matter how large the value of \dot{M} reaches, the escaping luminosity approaches a straight line, similar to the one shown with a red dashed curve in the inset of Figure 1. This is because as \dot{M} increases the timescale for shock-powered radiation to diffuse out of the equatorial outflow also increases. Eventually, once the diffusion time exceeds the expansion timescale and the timescale over which \dot{M} increases, this limits the rate at which the light curve can rise in the simulations.

We find that the observed upward curvature of the light curve can be explained if we assume that the initial temperature T_{in} of the L_2 mass loss also increases with \dot{M} , as shown with a red solid line in the inset of Figure 1. We parameterize the temperature increase according to Equation (10), where we take values $\dot{M}_0 = 10^{-3} M_{\odot} \text{ yr}^{-1}$, singularity t_0 positioned 200 days after the start of the simulation, $\delta = 3$, $\dot{M}_T = 10^{-2} M_{\odot} \text{ yr}^{-1}$, and $\gamma = 0.5$. Not being the result of a rigorous fit, these parameters are probably degenerate to some extent, but limited computational resources precluded us from exploring the parameter space more completely. The temporal evolution of quantities of interest, such as \dot{M} , the total mass loss, and the degree of binary asynchronism, are shown in Figures 7 and 8. The overall mass-loss history prior to the main peak is visualized in Figure 5. Our calculations suggest that V1309 Sco lost a total of $0.05 M_{\odot}$ prior to the main peak. A movie showing the evolution of the L_2 outflow structure in the final ~ 200 days is available online (see the animated version of Figure 6).

We explored a number of alternative scenarios to explain the observed accelerating brightening before the main peak, but none were found to work. For instance, changes in the bolometric correction as the effective temperature of the equatorial outflow increases with growing \dot{M} are insufficient to explain the upturn of the flux. As the binary becomes tighter, the velocity of the L_2 increases in proportion to the orbital velocity; however, the total budget of angular momentum and mass in the binary does not allow the later faster ejecta to overtake the earlier slower material at radii where the collision could efficiently radiate the dissipated energy (a process that would already be accounted for in our simulations). Mass loss from the secondary could also reduce the binary mass ratio q below the critical value of $\lesssim 0.064$, at which the L_2 outflow is expected to transition from a comparatively radiatively inefficient narrow equatorial outflow to a more radiatively efficient accretion disk or isotropic wind (Pejcha et al. 2016b). However, the initial mass of the secondary would need to be fine-tuned to achieve this transition at just the right time to generate the required luminosity.⁹ Using dust-free opacity tables only shifts the problem to somewhat higher values of \dot{M} .

Our code eventually crashes, and we are unable to follow the evolution any further. Figure 7 shows that this happens when the semimajor axis and orbital period have decreased to about a third or fifth of their original values, respectively. Since the mass ratio does not change appreciably, the orbital angular

momentum has also decreased to about the third of its original value by this point. About 10 days after the termination of our simulation, V1309 Sco underwent its final dynamical phase and concomitant brightening to maximum. It is thus tempting to speculate that the final dynamical interaction was a direct consequence of the nearly complete loss of the binary angular momentum by the prolonged L_2 outflow. However, without a direct simulation of the evolution of the binary structure itself, we cannot definitively prove a causal link.

This speculation, however, gives an observably testable prediction: to remove the orbital angular momentum from the system, the binary needs to lose about 10%–30% of the mass of the lighter star by L_2 outflow (MacLeod et al. 2017). Part of the uncertainty in the total mass lost comes from ambiguity in assigning the mass loss to either of the stars in the binary (Pribulla 1998). Furthermore, the mass loss rate culminates in the final 10–20 orbital revolutions, when the binary might not be able to maintain corotation with the orbit, even in its surface layers. Mass lost during this phase would thus carry lower specific angular momentum than that of L_2 in corotation, which would require a higher amount of mass to be lost. Nonetheless, many transients similar to V1309 Sco show evidence of secondary peaks that can be explained by shock interaction of dynamical ejecta, with an equatorially focused pre-existing material containing about 10% of the binary mass (Metzger & Pejcha 2017). In principle, more detailed modeling of the transient light curves and spectra can be used to constrain the quantity of pre-dynamical mass loss in the equatorial outflow.

4.2. Interpretation of the Increase of T_{in}

As described in Section 4.1, the most plausible scenario we find to explain the accelerating brightening of V1309 Sco in early 2008 is that, in addition to the rising value of \dot{M} , the temperature T_{in} at which matter is ejected at L_2 must increase secularly as well. As a result of the rising temperature, the spiral stream becomes progressively wider, the self-collision occurs closer to the binary, and the radiative efficiency $L_{\text{stream}}/\dot{M}$ increases (Pejcha et al. 2016a).

Although a changing bolometric correction is insufficient to explain the accelerating brightening in the I band on its own, it can contribute more significantly to the evolution if T_{in} increases. However, as a corollary, any implications derived based on the I band flux alone will be highly uncertain, because the bandpass now likely resides on the blue exponential tail of the black body, and the flux is therefore extremely sensitive to the effective temperature, which we estimate relatively crudely. For this reason, we show only the bolometric luminosity predicted by our model in Figure 1.

4.2.1. Response of a Star to Mass Loss

There are two fairly natural reasons why the value of T_{in} could increase approaching the terminal stages of the merger. First, as the binary loses mass, hotter layers below the surface become exposed. Using Modules for Experiments in Stellar Astrophysics (MESA) version 8118 (Paxton et al. 2011, 2013, 2015), we perform numerical calculations to explore the appearance of the star subjected to constant hydrodynamic mass loss. The numerical setup mostly follows previous work (Passy et al. 2012), but we choose the ‘‘Macdonald’’ equation of state to obtain a smoother evolution. We evolved a star according to MESA’s ‘‘1M_pre_ms_to_wd’’

⁹ Our final simulation, shown in Figure 1, evolves to $q < 0.064$ only in the last day or so, which is too late to appreciably affect the radiative properties.

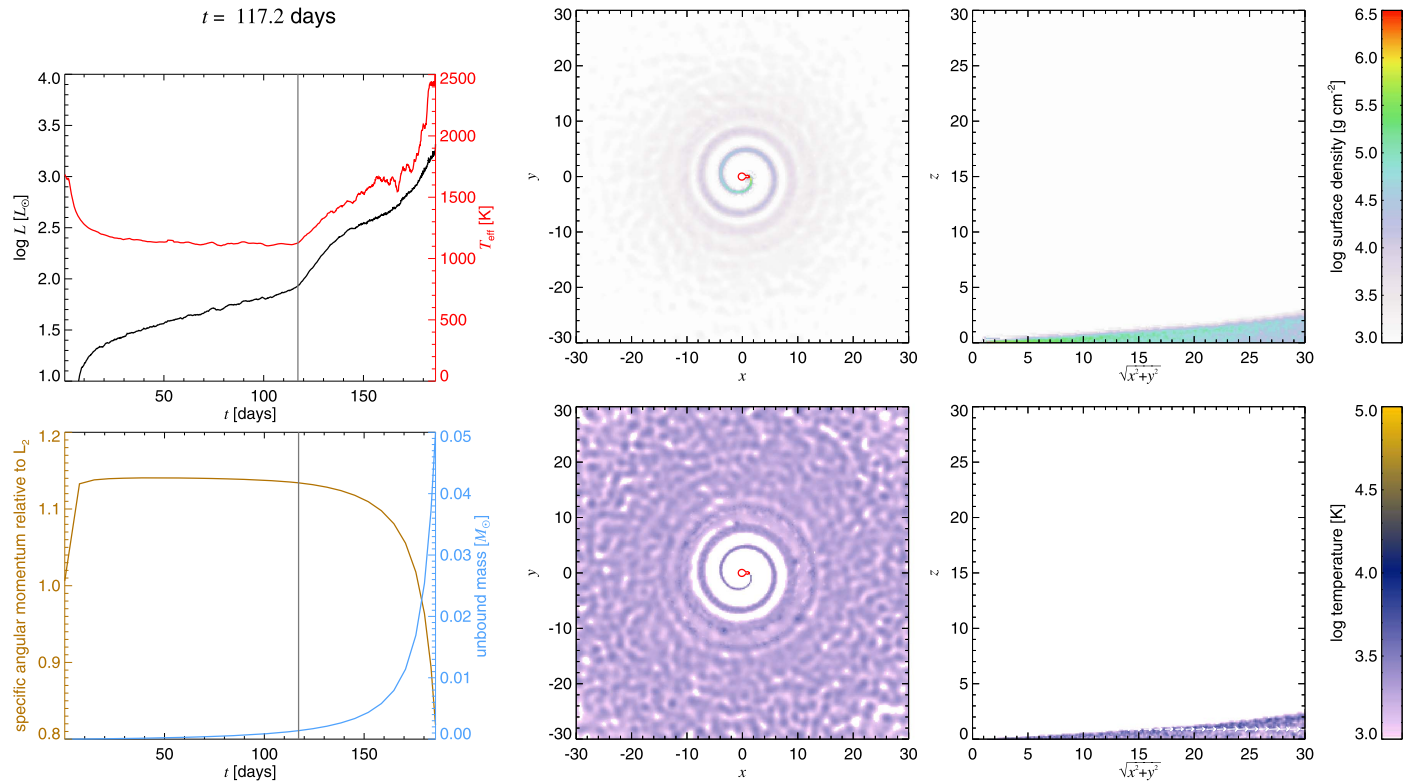


Figure 6. Online animated figure showing the evolution of the L2 outflow structure in the final 200 days. The right four panels show the evolution of density and temperature projected in the orbital plane and in the $\sqrt{x^2 + y^2} - z$ plane. The left top panel shows luminosity and estimated effective temperature (see Pejcha et al. 2016a, 2016b for details). The bottom left panel shows total mass lost from the binary (prescribed by $\dot{M}(t)$) and the specific angular momentum relative to L_2 at the beginning of the simulation. During the simulation, the binary orbit shrinks, and progressively more mass is ejected with smaller angular momentum, which leads to a decrease of the specific angular momentum measured in this way.

(An animation of this figure is available.)

test suite and saved a snapshot when the radius reached $10R_\odot$ after the main sequence. This procedure should roughly recover the structure of the heavier star, which is slightly inconsistent with the assumption of mass-loss coming from the lighter star (Section 2). However, we do not know which star is the source of the mass, and the two stars share their surface layer, where the heavier star probably dominates (at least for energy generation).

The saved model was then subject to constant hydrodynamic mass loss using “mass_change” control. The mass-loss rates we study probe the dynamical response of the star, where the thermal timescale is much longer than the mass-removal timescale. The maximum timestep was set to be smaller than the dynamical timescale of the star to properly resolve the transient pulsations. Although the details of the radius evolution depend sensitively on resolution and other numerical parameters, we find that the evolution of effective temperature is relatively robust. After the removal of mass commences, the effective temperature (and luminosity) of the star rise and asymptote to nearly constant value within ~ 1 day. These asymptotic values are nearly power-law functions of \dot{M} , with a kink in the dependence at around 10^4 K due to hydrogen ionization. Figure 8 shows the asymptotic effective temperatures as a function of time using the evolution of $\dot{M}(t)$ that we infer for V1309 Sco. The luminosities follow a similar trend as the temperature, because the fractional change in the radius is relatively small.

A similar increase in the effective temperatures and luminosities due to dynamical-timescale mass loss was reported

previously (Passy et al. 2012; Pavlovskii & Ivanova 2015). We caution that this behavior differs from the more commonly investigated thermal timescale mass loss, which leads to the dimming of the mass-losing star, because the thermal energy is expended on radial expansion (e.g., Gotberg et al. 2017). Furthermore, such high mass loss rates push 1D stellar evolution codes such as MESA near or beyond their design limits. Without further verification, our results on effective temperatures and luminosities should be regarded as only qualitative.

Although no color information is available during the last ~ 200 days prior to the peak of V1309 Sco, it appears unlikely that the gradual brightening in the first 8 months of 2008 is simply the result of heating of the binary surface without additional reprocessing by an external medium. First, the binary surface is no longer visible, as evidenced by the lack of variability during this time. In addition, similar gradual brightening phases observed in other stellar merger transients such as M101 OT2015-1 (Blagorodnova et al. 2017) suggest that the effective temperature decreases relative to the progenitor during this phase, implying a much larger photospheric radius.

4.2.2. Shearing Motions within the Contact Binary

Alternatively, gas leaving the binary could be pre-heated by the energy dissipated by shearing motions within the binary, due to a moderate loss of corotation. Similar possibility together with ejection of hotter layers was also mentioned by

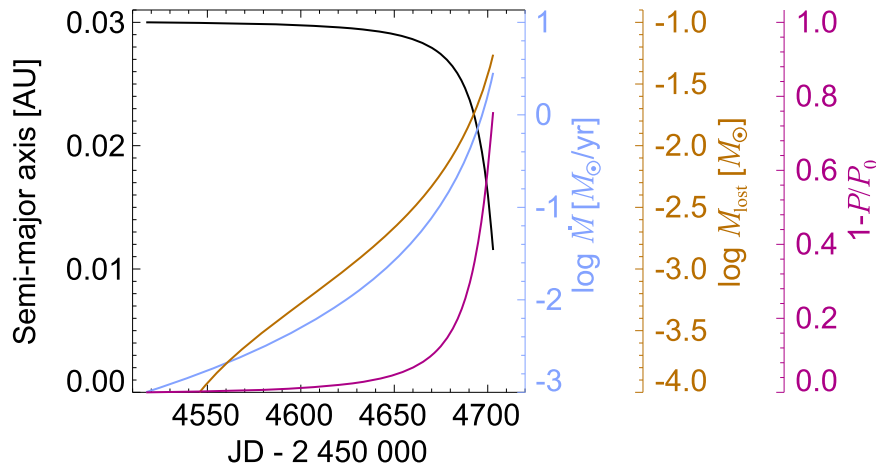


Figure 7. Evolution of binary properties that reproduce the observed gradual accelerating rise seen in Figure 1. Quantities shown include the semimajor axis a , the mass-loss rate \dot{M} , the total mass lost M_{lost} , and the degree of asynchronism $1 - P/P_0$.

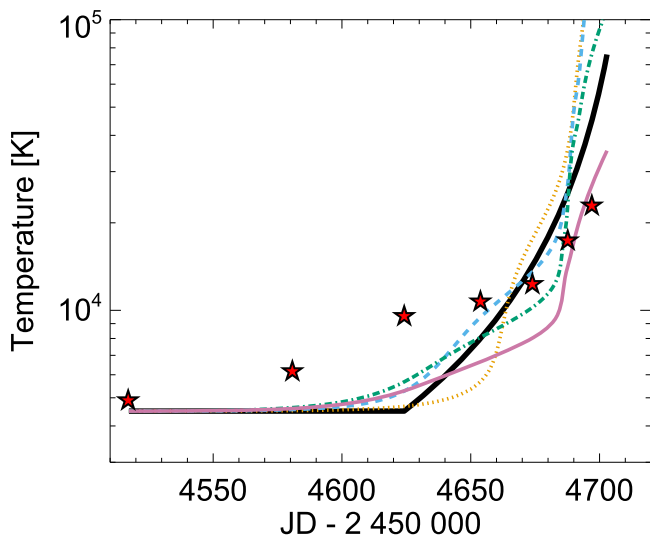


Figure 8. Time evolution of the injection temperature of matter at L_2 (black solid line) in comparison to our heuristic guess of its value due to frictional heating in the stellar envelope (colored lines). The latter are determined by first using our equation of state to find internal energy corresponding to the binary surface temperature, for different assumptions of the density at which the energy is deposited: $\rho = 10^{-4}$ (orange dotted), 10^{-6} (blue dashed), 10^{-8} (green dotted-dashed), and 10^{-10} g cm^{-3} (pink triple-dotted-dashed). Although the surface density of a $10 R_\odot$ subgiant from Section 4.2.1 is within the assumed range, our choice of density range but merely serves the point of illustrating that the results do not depend much on the density. Then, adding the approximate rate of frictional energy deposition $\Delta v^2/2$, where $\Delta v = (1 - P/P_0)v_{\text{orb},0}$ is the velocity shear due to desynchronization based on the observed evolution of V1309 Sco (Figure 7), we interpolate back to find the new surface temperature. Wiggles in the lines result from the ionization of hydrogen and helium. Stars show for comparison the predictions for the evolution of the effective temperature of a single non-rotating evolved star of mass $1 M_\odot$ and radius $10 R_\odot$, which is subject to the inferred mass loss history shown in Figure 7.

Kashi and Soker (2017). The observed period evolution of V1309 Sco proceeded so rapidly that the cores of the two contact binary components could not maintain synchronicity with the orbit (Tylenda et al. 2011). This results in a shearing layer between the two stars (Tylenda et al. 2011) with a velocity differential of the order of $\Delta v \sim (1 - P/P_0)v_{\text{orb},0}$ (Figure 7), where P_0 is the orbital period at the last moment when cores and envelopes were corotating (assumed to be the beginning of the OGLE data set), and $v_{\text{orb},0} = \sqrt{GM/a_0}$ is the

corresponding orbital velocity. Energy can be efficiently transported from the shearing layer to the surface by convection, and in steady-state the specific internal energy of the gas will be increased by $\sim \Delta v^2/2$ if adiabatic and radiative losses can be neglected. Our results in Figure 8 show that this heating can appreciably increase the surface temperature in the last ~ 100 days (~ 70 orbits) prior to the dynamical event. This process was likely accompanied by magnetic field generation or amplification, which is of potential interest (e.g., Tout et al. 2008; Ohlmann et al. 2016; Schneider et al. 2016). In a fraction of similar cases, the magnetic field generated in this way could potentially play a role in launching jet-like outflows that are observed in some planetary nebulae (e.g., Sahai & Trauger 1998; Bollen et al. 2017).

The existence of shear heating within the binary is not necessarily in conflict with the assumption of corotation at L_2 inherent to our SPH simulations. If the shearing is restricted to sub-synchronously rotating cores, the small amount of material in the envelope shared by the contact binary (with relatively little inertia) could still be forced to corotate with the orbit. If matter launched from near L_2 is not in corotation with the orbit, then tidal torquing might be less efficient, and mechanical interaction with the binary could heat the gas and contribute to its outward acceleration.

5. Discussion and Conclusions

We have argued that the pre-maximum photometric evolution of V1309 Sco observed in detail by OGLE can be explained as a consequence of L_2 mass loss with progressively increasing mass loss rate. Initially, the resulting stream of gas is transparent, and its effects could be seen only in the orbital period evolution, possibly on top of other effects such as the Darwin instability. When the stream becomes semi-transparent, it begins to modify the phased light curve, and eventually the double-hump profile arising from mirror symmetry along the binary axis is replaced by a single-hump profile (Figure 2). The mass loss rates estimated from the phased light curves roughly match the simultaneous decay in orbital period (Figure 5), although there exist degeneracies between the mass-loss rate, inclination, opacity, and density profile of the outflow.

As mass-loss rate increases even further, the binary becomes obscured and the observer sees only the spiral collisions in the L_2 outflow. Extrapolating the runaway trend of \dot{M} increase, we

can reproduce the observed accelerating brightening to the maximum (Figure 1), provided that the particle injection temperature in the final ~ 100 days increases and raises the radiative efficiency of the outflow. Our results imply that V1309 Sco lost a total of $\approx 0.05 M_{\odot}$ over the last few thousand orbits before the final dynamical mass ejection. The total amount of mass lost is comparable to what hydrodynamical simulations predict for the subsequent dynamical phase (Ivanova et al. 2013a; Nandez et al. 2014). The timescale of L_2 mass loss is much longer than suggested by contemporary hydrodynamical simulations, for which the initial mass ejection occurs almost instantly and might be followed by a prolonged period of mass loss (e.g., Lombardi et al. 2011; Nandez et al. 2014; Clayton et al. 2017).

What are the prospects of observing the full evolution of a merging binary system similar to V1309 Sco again in the future? The OGLE data suggest that when L_2 mass loss sets in, the runaway lasts at most in a few thousand orbits, corresponding to a few years for short-period binaries. Before this phase, the binary might be relatively inconspicuous in photometric data sets. The frequency of stellar mergers in the Milky Way is roughly once every decade (Kochanek et al. 2014), thus implying that only a few binaries are undergoing accelerating period change in the entire Milky Way at any given time. Given this fact, it seems unlikely that a similar event is happening in the *Kepler* field, as reported in KIC 9832227 (Molnar et al. 2017). Furthermore, the reported mass ratio of this system seems too high for the tidal Darwin instability. Instead, this binary likely falls in the tail of the period change distribution observed in contact binaries, due to additional orbiting bodies in the system, stellar spots, or mass transfer effects (Pietrukowicz et al. 2017).

For binaries observed from inclinations smaller than $\sim 70^\circ$, the observer’s sight line will not intersect the L_2 mass loss stream. In such cases, the separate contributions to the observed flux from the binary and the shock-heated L_2 outflow should simply add together. This leads to the prediction of a gradually rising light curve without a major dip or early onset of asymmetry in the phased light curve. Unfortunately, a smaller inclination angle also reduces the amplitude of the binary variability, making the discovery of such a system in archival data challenging. For binaries viewed closer to edge-on, the dust formation in the equatorial outflow could potentially hide the central binary and the spiral shocks at very early times. The object would then become optically visible again only after the release of the more spherical dynamical ejecta. This is similar to the “Type II ILOT” of Kashi and Soker (2017). In systems similar to V1309 Sco, this would happen only for a narrow range of inclinations $i \gtrsim 85^\circ$, but the actual threshold depends sensitively on the density profile of the L_2 stream.

The origin of the rising temperature of the gas being injected from L_2 , which from our simulations we find is required to explain the accelerating brightening to the main peak (Figure 8), is unclear. It might be connected to the mass stripping of the surface layers or additional heating due to internal shears within the binary. Whatever its nature, our results suggest this heating process operates at least for many tens of orbits prior to the dynamical phase. We further speculate that the entirety of the runaway process observed in V1309 Sco could be “self-regulated,” in the sense that the evolution $\dot{M}(t)$ is determined by the expansion of the stellar radius, which is driven by shear heating, which in turn is

determined by the integrated history of mass loss and period decay. In this picture, the late-stage self-observed binary might appear very different than at earlier times (Figure 2), with strong surface flows/convection, mass ejection, and perturbations to the mass loss stream. This complex behavior is captured only heuristically in our simulations by increasing T_{in} , but direct time-dependent multi-dimensional simulations of this phase are unfortunately challenging due to long timescales and complex physical processes (e.g., convection, radiative transport). Even the time-steady structure of contact binary envelopes remains an unsolved problem (Shu & Lubow 1981; Kähler 2004; Eggleton 2006; Rucinski 2015).

What triggered the ultimate dynamical event in early 2008 September? Our requirements on the mass loss needed to explain the slow brightening phase prior to this point show that the dynamical transition occurs at roughly the point when an order unity fraction of the binary’s total original angular momentum has been lost through L_2 . We thus hypothesize that reaching this critical point—at which the stellar cores have become sufficiently close to interact directly—was responsible for initiating the final dynamical coalescence and its concomitant mass ejection.

Our models show that roughly $0.05 M_{\odot}$ was lost from the binary prior to the dynamical event, an amount of mass comparable to the quantity $0.04\text{--}0.09 M_{\odot}$ needed to explain the main light curve peak and subsequent plateau (Ivanova et al. 2013a; Nandez et al. 2014). The mass ejection that occurs promptly during the dynamical phase is expected to be faster and approximately isotropic in geometry (Tylanda et al. 2011), in which case it will drive a shock through the earlier L_2 outflow accumulated primarily along the orbital plane. The shock will soon be engulfed within the more spherical recombining ejecta, with additional heating from the shocked shell acting to lengthen the duration of the hydrogen recombination plateau (Metzger & Pejcha 2017), similarly to radioactive nickel decay or magnetar spindown in SNe II (Kasen & Woosley 2009; Sukhbold & Thompson 2017). Conversion of shock kinetic energy to radiation is most efficient when the masses in the two colliding media are similar, as we find appears to be the case for V1309 Sco. We illustrate this scenario qualitatively in Figure 9, where we initiate a spherical explosion inside the equatorial density structure assembled during the pre-maximum evolution of V1309 Sco.

The collision of spherical fast ejecta with a slower equatorial outflow naturally leads to double-peaked light curves, as observed in many transients in the class similar to V1309 Sco (Metzger & Pejcha 2017), and this suggests that stellar binary mergers commonly lose significant mass well before the dynamical phase. If the dynamical event results in a similar total mass ejection as the preceding equatorial L_2 phase ($\sim 10\%$ of the total binary mass), then the resulting shock interaction can explain the observed range of luminosities and durations of transients from binary interactions. Depending on the shock energy set by the binary parameters, the collision might not be energetic enough to keep the hydrogen in the fast expanding shell ionized, and there would not be a second peak. Metzger and Pejcha (2017) suggest that this indeed might be the case for V1309 Sco and perhaps also M31 LRN 2015 (Kurtenkov et al. 2015; Williams et al. 2015). If the shock cannot prevent dust formation, which should occur more readily in long-period

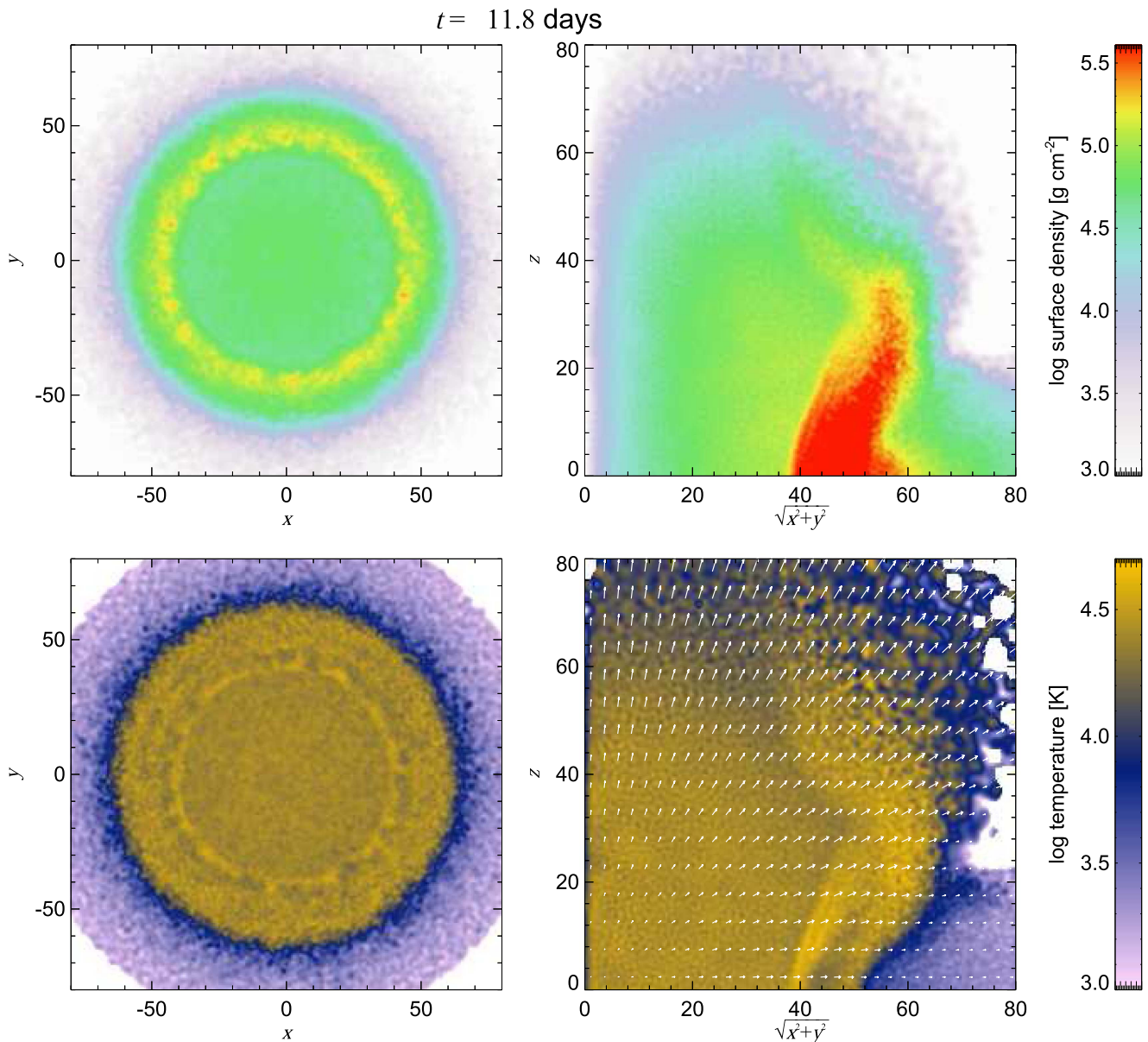


Figure 9. Density and temperature structure of the collisions of faster spherical ejecta with pre-existing equatorial L_2 outflow. The two left panels show density and temperature of particles projected in the orbital plane, while the two right panels show the same quantities in the $\sqrt{x^2 + y^2} - z$ plane. The initial condition for the equatorial component is the final snapshot from the simulation of gradual brightening of V1309 Sco (inset of Figure 1). The spherical explosion was initiated by positioning a stationary ball of hot particles in a sphere centered on the binary barycenter, similarly to Metzger and Pejcha (2017). Gravitational forces and radiative diffusion and cooling were not included in this calculation. The swept-up shell in the equatorial plane fractures into clumps due to hydrodynamical instabilities. The formation of such a clumpy ring can be obtained in different settings, such as a propagation of a jet into a spherical shell (Akashi et al. 2015).

(An animation of this figure is available.)

binaries with more evolved components, the forming dust will shift the peak of the spectral energy distribution to the infrared and prolong the transient duration. This provides an explanation for some members of the recently identified class of infrared transients known as SPRITEs, which have durations of hundreds of days to years and luminosities in the gap separating classical novae and supernovae (Kasliwal et al. 2017). It is currently unclear what fraction of the binary mass is ejected in these events, but SPRITEs may represent mergers in which the outcome is a binary surviving on a tighter orbit (the classical definition of a “common envelope”). Transients identified at optical wavelengths, including V1309 Sco, appear to originate from more compact

progenitors, in which case most of the envelope is retained, leading to a complete merger.

Modeling transient events in their entirety, including the early slow rise phase studied here, offers a new avenue to explore the progenitor binaries, probe binary stability across a wide range of stellar properties, reduce uncertainties in binary population synthesis models, and provide realistic initial conditions for multi-dimensional numerical simulations of the dynamical phase.

V1309 Sco remains enshrouded in dust, making direct proof of a single-star remnant challenging to obtain. The bolometric luminosity of the remnant is significantly higher than prior to the outburst (Tylenda & Kamiński 2016). If the merger

remnant is a single star, it is undergoing thermal relaxation. Its long-term light curve will encode information on the energy and angular momentum injected into the star, as probed by the directly observed dynamical phase of the merger. With new data coming from time-domain surveys from ground and space, including *Gaia*, now is an opportune time to explore the full range of signatures of catastrophic interactions in binary star populations (Rucinski 2001).

O.P. is currently supported by Primus award PRIMUS/SCI/17 from Charles University. In the past, O.P. was supported by program number HST-HF-51327.01-A, provided by NASA through a Hubble Fellowship grant from the Space Telescope Science Institute, which is operated by the Association of Universities for Research in Astronomy, Inc., under NASA contract NAS5-26555, and in part by the National Science Foundation under Grant No. NSF PHY-1125915 to KITP. B.D.M. acknowledges support from the National Science Foundation (AST-1615084) and NASA Astrophysics Theory Program (NNX16AB30G, NNX17AK43G). We thank Ronald Taam for comments on the early version of the manuscript. We thank the referee for comments that helped improve the paper.

ORCID iDs

Ondřej Pejcha  <https://orcid.org/0000-0003-2512-2170>
Kengo Tomida  <https://orcid.org/0000-0001-8105-8113>

References

- Abbott, B. P., Abbott, R., Abbott, T. D., et al. 2016a, *PhRvL*, **116**, 241102
 Abbott, B. P., Abbott, R., Abbott, T. D., et al. 2016b, *PhRvL*, **116**, 241103
 Abbott, B. P., Abbott, R., Abbott, T. D., et al. 2017, *PhRvL*, **118**, 221101
 Akashi, M., Sabach, E., Yogeve, O., & Soker, N. 2015, *MNRAS*, **453**, 2115
 Alexander, D. R., & Ferguson, J. W. 1994, *ApJ*, **437**, 879
 Blagorodnova, N., Kotak, R., Polshaw, J., et al. 2017, *ApJ*, **834**, 107
 Bollen, D., Van Winckel, H., & Kamath, D. 2017, arXiv:1708.00202
 Clayton, M., Podsiadlowski, P., Ivanova, N., & Justham, S. 2017, *MNRAS*, **470**, 1788
 Eggleton, P. 2006, in *Evolutionary Processes in Binary and Multiple Stars*, ed. P. Eggleton (Cambridge: Cambridge Univ. Press)
 Flannery, B. P., & Ulrich, R. K. 1977, *ApJ*, **212**, 533
 Forgan, D., Rice, K., Stamatellos, D., & Whitworth, A. 2009, *MNRAS*, **394**, 882
 Gotberg, Y., de Mink, S. E., & Groh, J. H. 2017, arXiv:1701.07439
 Ivanova, N., Justham, S., Avendano Nandez, J. L., & Lombardi, J. C. 2013a, *Sci*, **339**, 433
 Ivanova, N., Justham, S., Chen, X., et al. 2013b, *A&ARv*, **21**, 59
 Kafka, S. 2017, Observations from the AAVSO International Database, <https://www.aavso.org>
 Kähler, H. 2004, *A&A*, **414**, 317
 Kasen, D., & Woosley, S. E. 2009, *ApJ*, **703**, 2205
 Kashi, A., & Soker, N. 2017, *MNRAS*, **467**, 3299
 Kasliwal, M. M., Bally, J., Masci, F., et al. 2017, *ApJ*, **839**, 88
 Kochanek, C. S., Adams, S. M., & Belczynski, K. 2014, *MNRAS*, **443**, 1319
 Kurtenkov, A. A., Pessev, P., Tomov, T., et al. 2015, *A&A*, **578**, L10
 Livio, M., Salzman, J., & Shaviv, G. 1979, *MNRAS*, **188**, 1
 Livio, M., & Soker, N. 1988, *ApJ*, **329**, 764
 Lombardi, J. C., Jr., Holtzman, W., Dooley, K. L., et al. 2011, *ApJ*, **737**, 49
 MacLeod, M., Macias, P., Ramirez-Ruiz, E., et al. 2017, *ApJ*, **835**, 282
 MacLeod, M., & Ramirez-Ruiz, E. 2015, *ApJ*, **803**, 41
 Mason, E., Diaz, M., Williams, R. E., Preston, G., & Bensby, T. 2010, *A&A*, **516**, A108
 Mauerhan, J. C., Van Dyk, S. D., Johansson, J., et al. 2017, arXiv:1702.00430
 Metzger, B. D., & Pejcha, O. 2017, *MNRAS*, **471**, 3200
 Meyer, F., & Meyer-Hofmeister, E. 1979, *A&A*, **78**, 167
 Molnar, L. A., Van Noord, D. M., Kinemuchi, K., et al. 2017, *ApJ*, **840**, 1
 Nandez, J. L. A., Ivanova, N., & Lombardi, J. C., Jr. 2014, *ApJ*, **786**, 39
 Ohlmann, S. T., Röpkke, F. K., Pakmor, R., Springel, V., & Müller, E. 2016, *MNRAS*, **462**, L121
 Paczyński, B. 1976, in *IAU Symp. 73, Structure and Evolution of Close Binary Systems*, ed. P. Eggleton, S. Mitton, & J. Whelan (Dordrecht: Reidel), **75**
 Paczyński, B., Sienkiewicz, R., & Szczygieł, D. M. 2007, *MNRAS*, **378**, 961
 Passy, J.-C., Herwig, F., & Paxton, B. 2012, *ApJ*, **760**, 90
 Pavlovskii, K., & Ivanova, N. 2015, *MNRAS*, **449**, 4415
 Pawlak, M., Graczyk, D., Soszyński, I., et al. 2013, *AcA*, **63**, 323
 Paxton, B., Bildsten, L., Dotter, A., et al. 2011, *ApJS*, **192**, 3
 Paxton, B., Cantiello, M., Arras, P., et al. 2013, *ApJS*, **208**, 4
 Paxton, B., Marchant, P., Schwab, J., et al. 2015, *ApJS*, **220**, 15
 Pejcha, O. 2014, *ApJ*, **788**, 22
 Pejcha, O., Metzger, B. D., & Tomida, K. 2016a, *MNRAS*, **455**, 4351
 Pejcha, O., Metzger, B. D., & Tomida, K. 2016b, *MNRAS*, **461**, 2527
 Pietrukowicz, P., Soszyński, I., Udalski, A., et al. 2017, *AcA*, **67**, 115
 Pojmanski, G. 1997, *AcA*, **47**, 467
 Pribulla, T. 1998, *CoSka*, **28**, 101
 Rasio, F. A. 1995, *ApJL*, **444**, L41
 Rasio, F. A., & Shapiro, S. L. 1995, *ApJ*, **438**, 887
 Rucinski, S. M. 1993, *PASP*, **105**, 1433
 Rucinski, S. M. 2001, *AJ*, **122**, 1007
 Rucinski, S. M. 2015, *AJ*, **149**, 49
 Sahaï, R., & Trauger, J. T. 1998, *AJ*, **116**, 1357
 Sana, H., de Mink, S. E., de Koter, A., et al. 2012, *Sci*, **337**, 444
 Schneider, F. R. N., Podsiadlowski, P., Langer, N., Castro, N., & Fossati, L. 2016, *MNRAS*, **457**, 2355
 Shu, F. H., Anderson, L., & Lubow, S. H. 1979, *ApJ*, **229**, 223
 Shu, F. H., & Lubow, S. H. 1981, *ARA&A*, **19**, 277
 Smith, N., Andrews, J. E., Van Dyk, S. D., et al. 2016, *MNRAS*, **458**, 950
 Soker, N., & Tylenda, R. 2003, *ApJL*, **582**, L105
 Soker, N., & Tylenda, R. 2006, *MNRAS*, **373**, 733
 Stamatellos, D., Whitworth, A. P., Bisbas, T., & Goodwin, S. 2007, *A&A*, **475**, 37
 Stepień, K. 2011, *A&A*, **531**, A18
 Sukhbold, T., & Thompson, T. A. 2017, *MNRAS*, **472**, 224
 Tout, C. A., Wickramasinghe, D. T., Liebert, J., Ferrario, L., & Pringle, J. E. 2008, *MNRAS*, **387**, 897
 Tylenda, R., Hajduk, M., Kamiński, T., et al. 2011, *A&A*, **528**, A114
 Tylenda, R., & Kamiński, T. 2016, *A&A*, **592**, A134
 Tylenda, R., Kamiński, T., Udalski, A., et al. 2013, *A&A*, **555**, A16
 Tylenda, R., & Soker, N. 2006, *A&A*, **451**, 223
 Webbink, R. F. 1976, *ApJ*, **209**, 829
 Webbink, R. F. 1977, *ApJ*, **211**, 881
 Webbink, R. F. 1984, *ApJ*, **277**, 355
 Williams, S. C., Darnley, M. J., Bode, M. F., & Steele, I. A. 2015, *ApJL*, **805**, L18